

Quantification of the wound healing using polarization-sensitive optical coherence tomography

Jung-Taek Oh

Institute for Medical Engineering
Wonju, Kangwon
Korea 220-842

Sang-Won Lee

Yonsei University
Biomedical Engineering Department
Wonju, Kangwon
Korea 220-710

Youn-Soo Kim

Ki-Beom Suhr

CnU Skin Clinic and CnU Skin Research
Laboratory
Daejeon, Korea 301-712

Beop-Min Kim

Yonsei University
Biomedical Engineering Department
Wonju, Kangwon
Korea 220-710

1 Introduction

Wound healing is a complex process that restores cellular and/or tissue structures and functions. It involves synthesis and remodeling of collagen fibers, which are structural proteins abundant throughout the body.^{1,2} Occasionally, the wound healing mechanism becomes abnormal and induces fibrosis, hypertrophic scars, and keloid formation that result from excessive proliferation of the collagen fibers. Therefore, monitoring the morphological changes of collagen fibers may lead to understanding of the pathophysiology and, ultimately, to prevention of these abnormal conditions. Especially for abnormal wound healing patients such as diabetics, evaluation of the healing process and application of proper intervention are crucial.

Noninvasive monitoring technologies for wound healing are thus important tools to aid clinicians and researchers who need safe ways to evaluate healing. Monitoring treatment response with invasive biopsy procedure is not an option because a biopsy causes wounds. Researchers monitored electrical skin impedance to measure reepithelialization during wound healing, and local oxygenation measurements were also used to evaluate the recovery of tissues noninvasively.^{3,4} However, these methods cannot provide information regarding the structural changes of collagen that play a significant role during wound healing.

Abstract. We use polarization-sensitive optical coherence tomography (PS-OCT) to monitor the wound healing process *in vitro* and *in vivo*, which are affected by various drugs. Five rabbit subjects are used for *in vitro* studies and another five are used for *in vivo* studies. The *in vitro* studies are conducted to compare the PS-OCT images with histopathology. For each subject, three biopsy lesions are created on each ear: one site is not treated (control); the second site is treated with sphingosylphosphorylcholine, which is expected to promote healing; and the last is administered with tetraacetylphytosphingosine, which negatively affects the healing process. Each site is examined with a PS-OCT system at 1, 4, 7, 10, and 14- days after wound generation. The variations of phase retardation values caused by the collagen morphology changes on wound sites are quantified for all cases. Our results suggest that PS-OCT may be a useful tool for visualization of collagen fiber regeneration and for quantification of various drug effects during the wound healing process. © 2006 Society of Photo-Optical Instrumentation Engineers. [DOI: 10.1117/1.2338826]

Keywords: PS-OCT; wound healing; collagen fiber; SPC; TAPS.

Paper 05288SSR received Sep. 30, 2005; revised manuscript received Apr. 30, 2006; accepted for publication May 22, 2006; published online Sep. 8, 2006.

Optical coherence tomography (OCT) is a relatively new noninvasive imaging modality that can image the cross-sectional structure of skin with high resolution (1 to 20 μm) by means of low coherence interferometry.⁵ Polarization-sensitive OCT (PS-OCT) is a more advanced imaging method that can provide not only the cross-sectional images, but also information regarding the polarization changes due to tissue birefringence. In normal skin, birefringence is attributed to the loose and interlaced meshwork of collagen fibers in the dermis. Therefore, the PS-OCT allow us to evaluate the wound healing process involving the local variations of structural integrity of collagen fibers noninvasively.⁶⁻⁸

In this study, we used the PS-OCT system to monitor the wound healing of the rabbit skin tissues. The experiment was designed to detect differences in collagen fiber regeneration under the presence of healing and antihealing drugs, sphingosylphosphorylcholine (SPC) and tetraacetylphytosphingosine (TAPS), respectively. Although both drugs are not clinically established agents for wound healing yet, these agents have been studied to control the speed of healing. SPC is reported to stimulate wound healing by various mechanisms including mitogenic effect, and TAPS is known to deter neovascularization, which is necessary for healing.^{9,10}

Because the PS-OCT is a noninvasive technique, the same wound sites can be studied at various times after surgery. For the *in vitro* study, the PS-OCT images were analyzed and the tissue birefringence was quantified. These data were later

Address all correspondence to: Beop-Min Kim, Dept. of Biomedical Engineering, Yonsei University, 234 maeji, Heungup, Wonju, Kangwon-Do 220-710 Republic of Korea; Tel: 82 33 760 2490; Fax: 82 33 766 2464

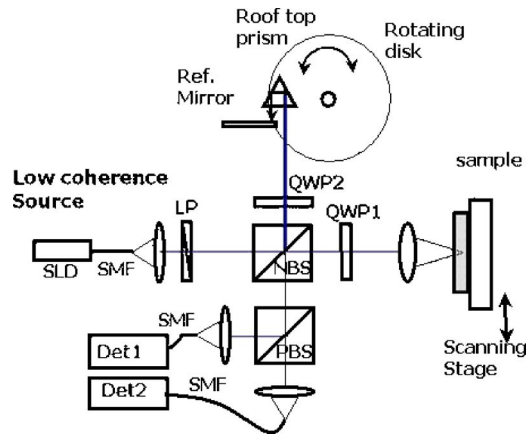


Fig. 1 Schematic of the bulk-type PS-OCT system. LP: linear polarizer, NBS: nonpolarizing beam splitter, PBS: polarization beam splitter, QWP: quarter wave plate.

compared with conventional histopathology. An *in vivo* study followed to analyze the same wound sites at various postoperative dates.

2 Materials and Methods

2.1 Sample Preparation

Ten adult white rabbits weighting between 3.5 and 4.0 kg were conditioned before our study. Three full thickness (about 0.5-mm depth) wound sites were made with biopsy punch (5-mm diameter) on each auricle skin of the rabbits so that the cartilage surfaces were exposed. Wounds were divided into three sets. One set was left untreated (control), and to each remaining set a different substance was applied topically immediately after wounding: SPC (5 μmol), TAPS (5 μmol). All wound sites were allowed to heal under transparent Duo-derm dressing. For the quantitative *in vitro* study, five rabbits were scarified just before PS-OCT imaging of wound sites on days 1, 4, 7, 10, and 14 postwounding. Therefore, we could obtain two PS-OCT images per animal for control, SPC, and TAPS at each time point. Biopsies were performed on each set of wounds after the imaging. All biopsy sections used for histology slides were selected to be close to the imaging section for the comparison. By referring to the same boundary marks for both imaging and the biopsy, we registered histology sections with the OCT images. The excised samples were stained with Mason trichrome, which is known to color the collagen blue. For continuous monitoring of the wound healing, another five rabbits were chosen. Each of them was individually imaged at 1, 4, 7, 10, and 14 days at the same wound sites with the PS-OCT system *in vivo*. Ten data points (two for each of five animals) for control, SPC, and TAPS at each time point were acquired.

2.2 PS-OCT Instrumentation for In Vitro Study

Figure 1 shows the schematic of the bulk-optics-type PS-OCT system used for the *in vitro* investigation. It is basically a partial coherence Michelson interferometer designed to detect the polarization state of backscattered light from tissues. Broadband light from a superluminescent diode (SLD) with a center wavelength of 1296 nm and full width at half maxi-

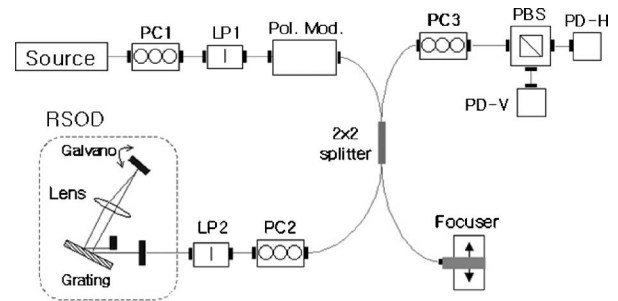


Fig. 2 Schematic of the fiber-based PS-OCT system. PC: polarization controller, PBS: polarization beam splitter, Pol. Mod.: polarization modulator.

um bandwidth of 40 nm is coupled into a linear polarizer (LP). After transmission through LP, a horizontal light is split into the sample and reference arms. Light in the reference arm passes through a quarter wave plate (QWP) oriented at 22.5 deg with respect to the horizontal axis so that the reflected light has a 45-deg linear polarization state after round trip. The QWP plate in the sample arm is oriented at 45 deg to horizontal to provide circularly polarized light to the sample. Light reflected from the skin is recombined with that from the reference arm, which then is split into two orthogonal polarization states. Lights are detected by two photodetectors and digitized by data acquisition board. The axial scanning rate is 20 Hz, and the axial and lateral resolutions are 18 μm and 14 μm , respectively. The power incident on the sample is 0.6 mW and the signal-to-noise ratio (SNR) is 96 dB. This slow scan speed helps us to obtain high quality OCT images, which we can then directly compared to the histology pictures. The Stokes parameters $[S_0(z)S_1(z)S_2(z)S_3(z)]$ are calculated from the two orthogonal polarized lights.⁶ A conventional OCT structure image is formed using intensity of backscattered light $S_0(z)$. A birefringence image constructed from $S_3(z)$ visualizes the birefringence tissue regions in the form of depth-resolved polarization change of light reflected from tissue. The rate at which the Stokes parameter $S_3(z)$ oscillates with depth is proportional to the magnitude of phase retardation ϕ . Therefore, the phase retardation angle can be calculated from the depth-resolved polarization changes. We obtained the quantitative information by calculating phase retardation as a function of depth.⁶

2.3 PS-OCT Instrumentation for In Vivo Study

Figure 2 is the schematic of the fiber-based PS-OCT system used for *in vivo* study. The basic principle of the system used in this study is the same as the previously described bulk-type PS-OCT system, but it was built to conduct a fast scanning of tissue for *in vivo* samples.¹¹ Briefly, light from SLD with a center wavelength of 1310 nm and bandwidth of 60 nm is passed through the polarization controller (PC1) and linear polarizer (LP1) to make linear polarized light with full power. Linear polarized light is sent to a piezodriven polarization modulator controlled by a four-step driving function designed to change into four orthogonal states in a Poincaré sphere representation. After passing through the polarization modulator, the light is split into the sample and reference arms by a 50/50 beam splitter. In the reference arm, PC2 and LP2 are

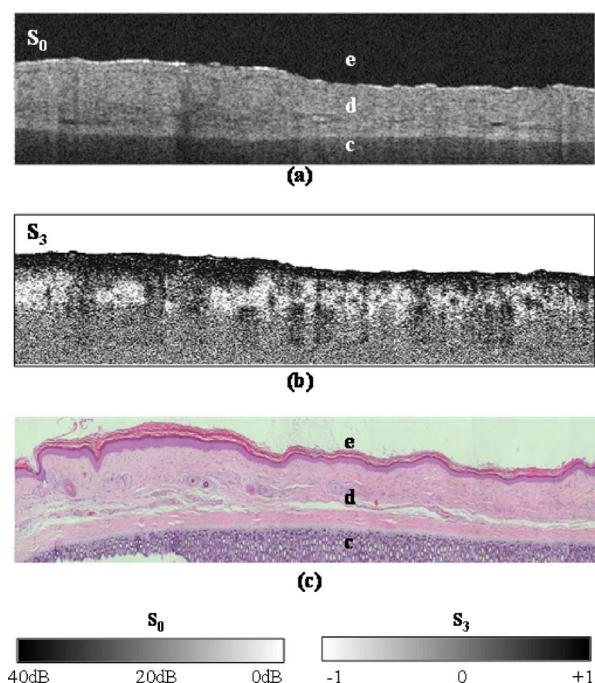


Fig. 3 PS-OCT images of normal auricle skin. (a) Backscattering intensity, (b) birefringence, and (c) the histology of a region nearby (H&E stained). The images are 1.3 mm (depth) \times 7.5 mm (width) in physical dimension. Epidermis, dermis, and cartilage are marked in (a), (c) as e, d, and c, respectively.

used to maintain the linear constant polarization state. We use the rapid scanning optical delay for depth scanning. In the sample arm, a linear piezomotor is attached to a focuser for B-scanning. Light reflected from the skin is recombined with light from the reference arm, which then is split into two orthogonal polarization states and detected by two photodetectors. The axial scanning rate and polarization-changing rate of the polarization modulator are 200 Hz and 50 Hz, respectively. The axial resolution is about 20 μm in air. The power incident on the sample is 0.9 mW and the SNR is 83 dB. We referred to Park et al. for obtaining phase retardation in birefringent tissue from the raw data.¹²

3 Results

A representative *in vitro* image of normal auricle skin is shown in Fig. 3 with the corresponding histology. The layered structure of skin composed of epidermis (e), dermis (d), and cartilage (c) is visible in backscattering intensity image [Fig. 3(a)]. The distinction between epidermis and dermis is more pronounced by corresponding birefringence image [Fig. 3(b)]. The gray level represents the cosine of the phase retardation. If the collagen density is high or collagen fiber orientation is parallel to the surface, the phase retardation angle changes rapidly with depth and the black and white strips appear repeatedly. There is a small birefringence change inside the epidermal layer as manifested by no gray level change, while the birefringence change within the dermal layers is clearly visible, as shown by the S_3 parameter (cosine of phase retardation angle) change from 1 to -1 (from black to white). The hematoxylin and eosin (H& E) stained histology image [Fig.

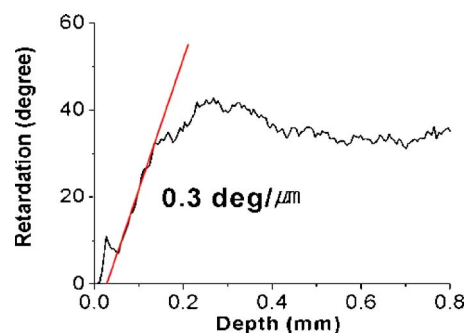


Fig. 4 Measured mean phase retardation of normal rabbit auricle skin.

3(c)] taken near the same region validates the layered structure in the auricle skin. Figure 4 shows the mean retardation values with depth over the full width of the image corresponding to Fig. 3(b). The graph indicates that the retardation values linearly increase from 0.05 mm to 0.2 mm from the surface, which is inside the dermis. The least-squared linear fits of the linear regions are used to quantify birefringence inside the dermis. The fitting line in Fig. 4 shows that the mean phase retardation is approximately 0.3 $\text{deg}/\mu\text{m}$ for normal auricle skin. This value is similar to that of human skin, which is known to be in the range of 0.25 to 0.6 $\text{deg}/\mu\text{m}$.¹³ It is difficult to obtain quantitative information behind the linear range because randomly distributed collagen fibers scramble the polarization state of the backscattered light. For this study, we used only the linear regions for the quantification of the wound healing process.

Figure 5 shows the representative *in vitro* results after 14 days postsurgery. The three sets of images are backscattering intensity (S_0) and birefringence (S_3) images of the control site, SPC site, and TAPS site, respectively. S_0 images show that the tissue volume between cartilage and surface inside the wound site is thicker than that in the no-wound region and that its thickness varied depending on the applied agent. This enlarged tissue volume for the SPC-treated tissue seems smaller than those for TAPS and control sites. Comparing the birefringence images, the birefringence by collagen fibers are better restored when SPC was applied, which is evident from the larger polarization change under the wound (rapid gray level change with depth). The white arrows inside the S_3 image of the SPC site indicate these regions. On the other hand, the birefringence image of the TAPS wounds show less pronounced collagen restoration. It seems that the control wound images have a different feature, which can be described as scattered spots of strong birefringence change. The measured mean phase retardation ϕ of each case supports our observation: 0.06, 0.10, and 0.04 $\text{deg}/\mu\text{m}$ for control, SPC, and TAPS sites, respectively, for wounds in Fig. 5.

The mean degree of wound healing was quantified for *in vitro* and *in vivo* samples at 4, 7, 10, and 14 days post-wounding. We measured mean phase retardation angles both inside the wounds and near no-wound regions from each image. The mean phase retardation angle inside the wound was estimated by averaging 150 axial scans (1.5-mm length) near the wound center, which was identified visibly, bounded by both wound edges. The same number of axial scans was used for investigation of no-wound regions from each image. Then

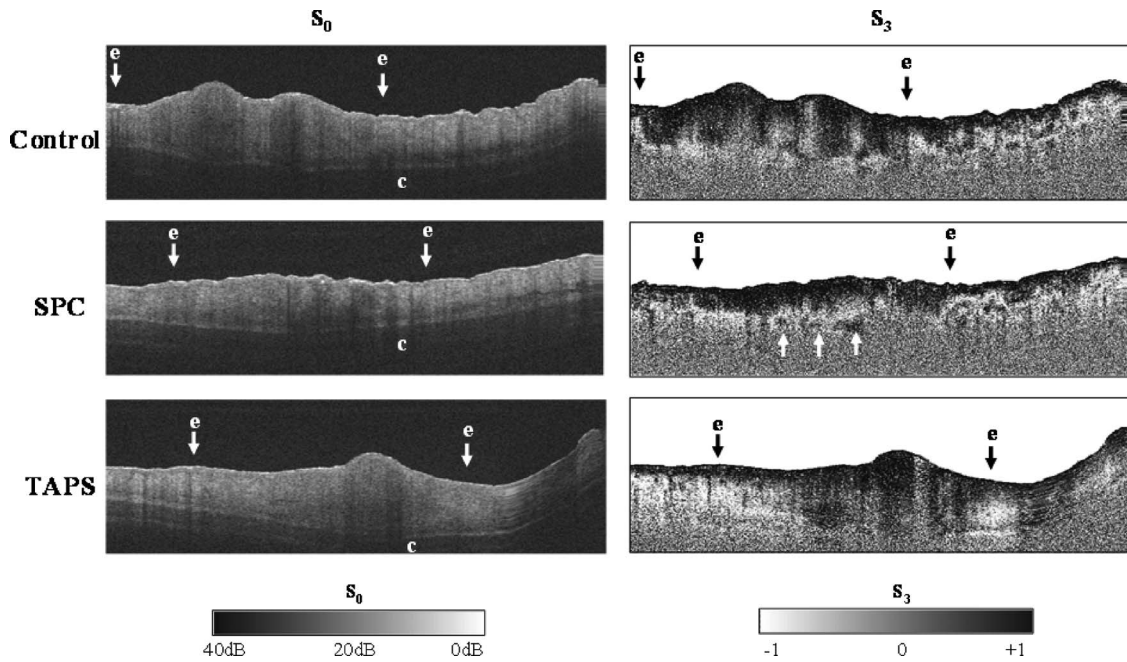


Fig. 5 PS-OCT images of day 14 postwounding. All images take the same color map drawn at Fig. 4. The physical size of each image is 1.3 mm (depth)×8.5 mm (width). Wound edges and cartilage are marked as e and c, respectively. Arrows point to wound boundaries. White arrows in the S_3 image for the SPC case indicate a region with rapid gray level change inside the wound healing region.

the mean phase retardation angle values of wound sites were normalized with those of no-wound regions to compensate for the individual difference of the samples. Therefore, if the normalized birefringence becomes close to the value of 1, it may mean that the collagen structure in the wound region is almost restored. The normalized phase changes (birefringence change) at various dates are shown in Fig. 6. For the *in vivo* case, five animals were imaged to acquire data, and the error bars in the graph represent the maximum and minimum values for each data set. Even if the error bars are large due to sample variations, the overall trend of *in vivo* and *in vitro* data show the same feature. First, the SPC-treated and the control wounds show increasing birefringence restoration with time,

while TAPS-applied wounds show no or negligible improvement. Second, drug effects start to be pronounced after 10 days postsurgery. Before 10 days postsurgery, all the samples show low mean phase retardations and drug effects were not obvious. After 10 days postsurgery, SPC-applied wounds start to have higher phase retardations than control wounds and reach almost to that of the nearby normal tissue in 14 days. Statistical analysis of the data in Fig. 6(b) supports the trends we found in both *in vivo* and *in vitro* experiments. Both *p* values for each agent at 14 days postsurgery indicate that the differences in mean phase retardations are statistically significant ($p < 0.05$).

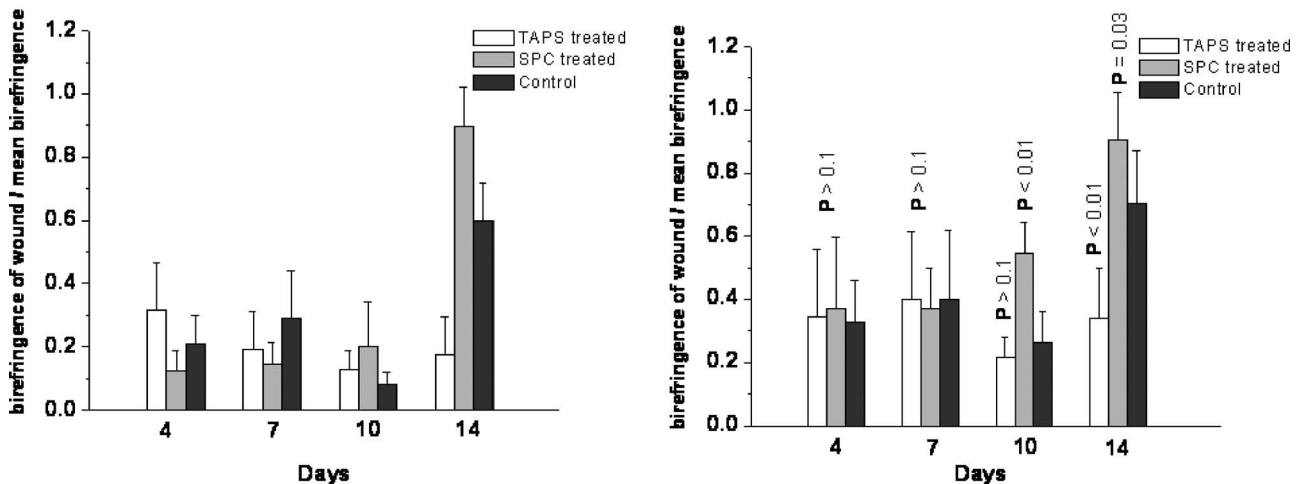


Fig. 6 The correlation between mean phase retardation and days postwounding: *in vitro* (a) and *in vivo* (b) cases. The error bars in the *in vivo* case represent the standard deviation of measured values for each data set.

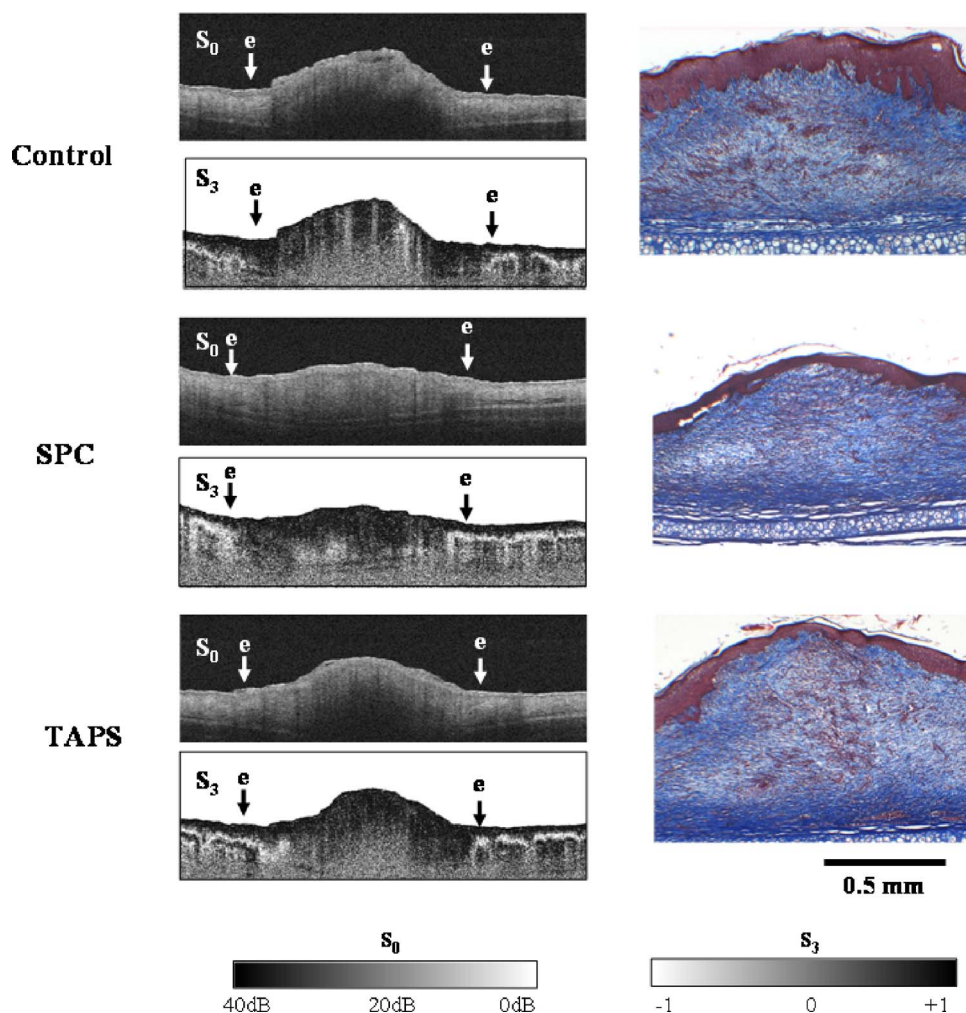


Fig. 7 PS-OCT images and the corresponding histology of day 10 postwounding: (a) PS-OCT images and (b) Mason trichrome stained histology. Each row of images is from the control, SPC, and TAPS sites, respectively. The physical size of each OCT image and histopathologic image is 1.3 mm (depth) \times 8.5 mm (width), 1.0 mm (depth) \times 1.5 mm (width), respectively. Wound edges are marked as e, and arrows point to wound boundaries.

It should be noted that the phase retardation is not only correlated to collagen content, but also to the orientation of collagen fibers.¹⁴ To identify the dominant source of mean phase retardation difference in the wound healing process, we compared some of our PS-OCT images with the corresponding histologies. The *in vitro* results at 10 days postsurgery and corresponding histologies are presented in Fig. 7. The left three sets of images are birefringence (S_3) images of control, SPC, and TAPS sites, respectively. The right column images are corresponding histology pictures with Mason trichrome staining, which selectively stains the collagen blue. The histology images show that the collagen fiber density is high for both SPC and control cases, and low in TAPS wound. Figure 8 shows the image-processed histology pictures that signify the orientation of collagen fibers. An image thinning process was applied to enhance the visualization of fiber orientation.¹⁵ Collagen fiber orientation maps of SPC-applied wounds indicate preferentially aligned fibers in parallel with the skin surface. On the contrary, randomly distributed fiber bundles are found in control and TAPS wounds. Therefore, it is concluded that SPC stimulated more and parallel collagen

generation, both of which contributed to the large phase retardation shown in the PS-OCT images.

4 Discussion

In this study, PS-OCT was used to quantify the healing process in terms of the phase retardation values in wounded skin to which either SPC or TAPS were topically applied. The results support the conclusion that the SPC-treated wounds have about 30% higher phase retardation than the control wounds ($P=0.03$), and the TAPS-treated wounds have 52% lower phase retardation than the control wounds ($P<0.01$).

SPC is known to be a wide modulator of the cells involved with wound healing including the upregulation of fibronectin that mediates collagen deposition and wound contraction, inducing alignment of fibers in granulation tissue.^{9,10} The observations of a larger amount of collagen fibers and the uniform orientation in the SPC site support the theory that the strong birefringence in PS-OCT images is caused by the accelerated healing process. Randomly distributed fiber bundles in TAPS-applied sites indicate that the drug does impede the healing

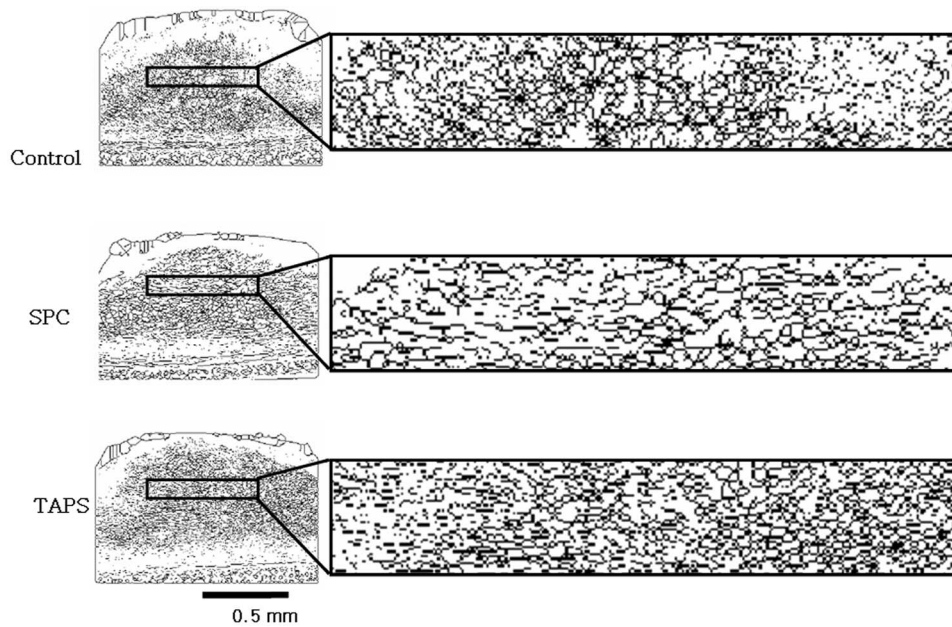


Fig. 8 Image-processed histology pictures of control, SPC-, and TAPS-treated wounds. The collagen fibers were selectively imaged. It is clear that the fiber directions in the SPC-treated wound are more parallel to the surface compared to the others.

process. The weak birefringence in the corresponding PS-OCT images can be explained by the same reason.

It is of interest to point out that our observation shown in Fig. 6 shows clear drug effects after 10 days postsurgery. Before 10 days postsurgery, all the samples display low mean phase retardations and drug effects were not distinguishable from each other. This specific timing of sudden change in phase retardation can be correlated to the healing phase. The entire wound healing process consists of four phases: hemostasis, inflammation, granulation tissue formation, and remodeling. Histopathologic findings of rabbit auricles showed that granulation tissues were markedly decreased and also showed signs of active collagen matrix remodeling, especially in SPC-treated sites at 10 days after wounding. Thus, our observation results support the conclusion that the quantification of the healing process by PS-OCT images reflects the progress of collagen matrix remodeling and its properties such as collagen contents and fiber orientation. Also, our results support that the SPC drug, which was known to improve the wound healing process, does so by optimizing the collagen remodeling process.

It is known that wound healing lasts for years after the initial injury occurred. In that period, collagen is degraded and deposited in an equilibrium-producing rate. Also, changes in collagen fiber orientation are expected. As a future study, we design long-term observations longer than 14 days to obtain complete views regarding changes of PS-OCT images through out the entire healing process.

5 Summary

In this study, we obtained the cross-sectional and polarization images of wounds by means of PS-OCT. Drug effects, such as acceleration or inhibition of the process, were noninvasively monitored using the system. Wound healing processes for two drugs that cause opposite effects were monitored, and distinc-

tive features were extracted from them. Based on *in vitro* and *in vivo* experiments, we found that the quantification of the degree of wound healing using PS-OCT images reflects the initiation of matrix deposition and its properties of collagen contents and fiber orientation. Our studies indicate that the PS-OCT system might be useful for studies related to abnormal wound healing and drug developments.

Acknowledgments

This research was supported by a Regional Research Center program that was conducted by the Ministry of Commerce, Industry, and Energy of the Korean government.

References

1. R. Clark, *Dermatology in General Medicine*, McGraw-Hill, New York (1996).
2. J. Gailit and R. Clark, "Wound repair in the context of extracellular matrix," *Curr. Opin. Cell Biol.* **6**, 717–725 (1994).
3. L. Adam, A. Tadmor, E. Aizinbud, and H. Schindler, "Electrical impedance monitoring of the wound-healing process," *Med. Prog. Technol.* **9**, 227–232 (1982).
4. F. Gottrup, "Oxygen in wound healing and infection," *World J. Surg.* **28**, 312–315 (2004).
5. D. Huang, E. A. Swanson, C. P. Lin, J. S. Schuman, W. G. Stinson, W. Chang, M. R. Hee, T. Flotte, K. Gregory, C. A. Puliafito, and J. G. Fujimoto, "Optical coherence tomography," *Science* **254**, 1178 (1991).
6. J. F. de Boer, T. E. Milner, and J. S. Nelson, "Determination of the depth-resolved Stokes parameters of light backscattered from turbid media by the use of polarization-sensitive optical coherence tomography," *Opt. Lett.* **24**, 300–302 (1999).
7. A. T. Yeh, B. Kao, W. G. Jung, Z. Chen, J. S. Nelson, and B. J. Tromberg, "Imaging wound healing using optics coherence tomography and multiphoton microscopy in an *in vitro* skin-equivalent model," *J. Biomed. Opt.* **9**, 248–253 (2004).
8. C. W. Han, C. R. Chu, N. Adachi, A. Usas, F. H. Fu, J. Huard, and Y. Pan, "Analysis of rabbit articular cartilage repair after chondrocyte implantation using optical coherence tomography," *Osteoarthritis Cartilage* **11**, 111–121 (2003).

9. Y. A. Hannun and R. M. Bell, "Function of sphingolipids and sphingolipid breakdown product in cellular regulation," *Science* **243**, 500 (1989).
10. H. J. Kim, H. J. Kim, S. C. Lim, S. H. Kim, and T. Y. Kim, "Induction of apoptosis and expression of cell cycle regulatory proteins in response to a phytosphingosine derivative in HaCaT human keratinocyte cells," *Mol. Cell* **16**, 331–337 (2003).
11. C. E. Saxer, J. F. de Boer, B. H. Park, Y. Zhao, Z. Chen, and J. S. Nelson, "High-speed fiber-based polarization-sensitive optical coherence tomography of *in vivo* human skin," *Opt. Lett.* **25**, 1355–1357 (2000).
12. B. H. Park, C. Saxer, S. M. Srinivas, J. S. Nelson, and J. F. de Boer, "*In vivo* burn depth determination by high-speed fiber-based polarization sensitive optical coherence tomography," *J. Biomed. Opt.* **6**, 474 (2001).
13. M. C. Pierce, J. Strasswimmer, B. H. Park, B. Cense, and J. F. de Boer, "Birefringence measurements in human skin using polarization-sensitive optical coherence tomography," *J. Biomed. Opt.* **9**, 287 (2004).
14. K. Kiraly, M. M. Hyttinen, T. Lapvetelainen, M. Elo, I. Kiviranta, J. Dobai, L. Modis, H. J. Helminen, J. Arokoski, and S. C. Tan, "Specimen preparation and quantification of collagen birefringence in unstained sections of articular cartilage using image analysis and polarizing light microscopy," *Histochem. J.* **29**, 317–327 (1997).
15. R. C. Gonzalez, R. E. Woods, and S. L. Eddins, *Digital Imaging Processing using MATLAB*, Prentice Hall, Upper Saddle River, NJ (2004).